Si IX EMISSION LINES IN SPECTRA OBTAINED WITH THE SOLAR EUV RESEARCH TELESCOPE AND SPECTROGRAPH (SERTS)

F. P. KEENAN[1], A. C. KATSIYANNIS[1], K. M. AGGARWAL[1], M. MATHIOUDAKIS[1], J. W. BROSIUS[2,3], J. M. DAVILA[2] and R. J. THOMAS[2]

[1]*Department of Pure and Applied Physics, The Queen's University of Belfast, Belfast BT7 1NN, Northern Ireland*

[2]*Laboratory for Astronomy and Solar Physics, Code 682, NASA's Goddard Space Flight Center, Greenbelt, MD 20771, U.S.A.*

[3]*Department of Physics, The Catholic University of America, Washington, DC 20064, U.S.A.*

(Received 9 July 2002; accepted 19 September 2002)

Abstract. Theoretical electron-density-sensitive emission line ratios involving $2s^2 2p^2$–$2s2p^3$ transitions in Si IX between 223 and 350 Å are presented. A comparison of these with an extensive dataset of solar-active-region, quiet-Sun, subflare and off-limb observations, obtained during rocket flights by the Solar EUV Research Telescope and Spectrograph (SERTS), reveals generally very good agreement between theory and experiment. This provides support for the accuracy of the line-ratio diagnostics, and hence the atomic data on which they are based. In particular, the density-sensitive intensity ratio I(258.10 Å)/I(349.87 Å) offers an especially promising diagnostic for studies of coronal plasmas, as it involves two reasonably strong emission lines and varies by more than an order of magnitude over the useful density range of 10^9–10^{11} cm^{-3}. The $2s^2 2p^2\ ^1S_0$–$2s2p^3\ ^1P_1$ transition at 259.77 Å is very marginally identified for the first time in the SERTS database, although it has previously been detected in solar flare observations.

1. Introduction

Emission lines arising from $2s^2 2p^2$–$2s2p^3$ transitions in carbon-like Si IX are frequently detected in solar ultraviolet spectra (Gallagher *et al.*, 1999, 2001). The usefulness of these lines as electron density (N_e) diagnostics for the emitting plasma was first noted by Mason and Bhatia (1978). Since then, several authors have produced theoretical line ratios for Si IX applicable to solar observations (see Keenan, 1996, and references therein).

In this paper we present new calculations of electron-density-sensitive line ratios for Si IX. We investigate the usefulness and accuracy of these diagnostics through a comparison with an extensive dataset of several quiet- and active-region spectra, plus a subflare and an off-limb area, obtained with the Solar EUV Research Telescope and Spectrograph (SERTS).

Solar Physics **212:** 65–79, 2003.

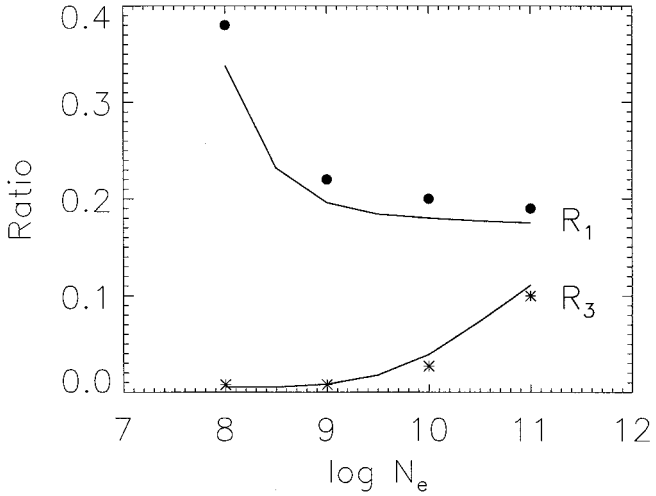

Figure 1. The theoretical Si IX emission line ratios $R_1 = I(223.74\ \text{Å})/I(349.87\ \text{Å})$ and $R_3 = I(259.77\ \text{Å})/I(349.87\ \text{Å})$, where I is in energy units, plotted as a function of logarithmic electron density (N_e in cm^{-3}) at the temperature of maximum Si IX fractional abundance in ionization equilibrium, $T_e = 1.25 \times 10^6$ K (Mazzotta *et al.*, 1998). The present calculations are shown as *solid lines*, while results from the CHIANTI Version 13 database are given as *filled circles* (R_1) and *stars* (R_3).

2. Theoretical Line Ratios

The model ion for Si IX consisted of the 9 energetically lowest LS states, namely $2s^2 2p^2\ ^3P$, ^1D, and ^1S, $2s2p^3\ ^5S$, ^3D, ^3P, ^1D, ^3S and ^1P, giving a total of 15 fine-structure levels. Energies for levels within $2s^2 2p^2$ were obtained from Brage *et al.* (2000), while those for $2s2p^3$ were obtained from Martin and Zalubas (1983). Test calculations including the higher lying $2p^4$ states were found to have a negligible effect on the theoretical line ratios involving $2s^2 2p^2 - 2s2p^3$ transitions considered in the present paper, demonstrating that cascades are not important here.

Electron impact excitation rates for $2s^2 2p^2 - 2s^2 2p^2$ transitions in Si IX were taken from Aggarwal (1983), all other data being obtained from Aggarwal (1984) and Aggarwal and Kingston (1986). For Einstein A-coefficients, the calculations of Brage *et al.* (2000) and Aggarwal (1998) were adopted for $2s^2 2p^2 - 2s^2 2p^2$ and $2s^2 2p^2 - 2s2p^3$ transitions, respectively. Proton impact excitation is only important for transitions among the $2s^2 2p^2\ ^3P$ levels, and in the present analysis we have employed the results of Ryans *et al.* (1999).

Using the atomic data discussed above in conjunction with the statistical equilibrium code of Dufton (1977), relative Si IX level populations and hence emission line strengths were calculated as a function of electron temperature (T_e) and density (N_e). Details of the procedures involved, and approximations made, may be found in Dufton (1977) and Dufton *et al.* (1978).

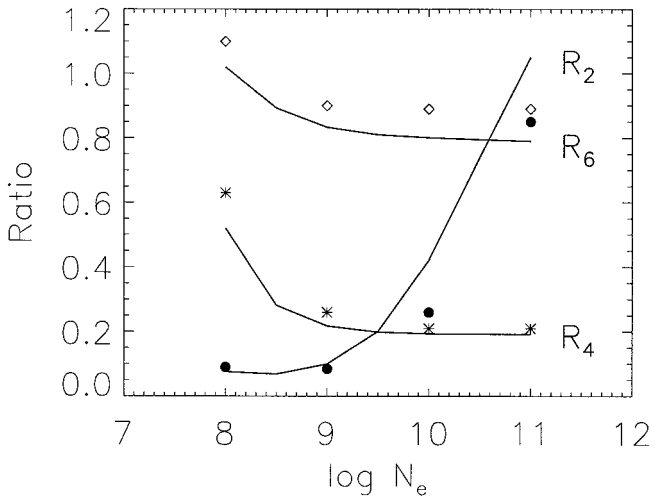

Figure 2. The theoretical Si IX emission line ratios $R_2 = I(258.10\ \text{Å})/I(349.87\ \text{Å})$, $R_4 = I(290.69\ \text{Å})/I(349.87\ \text{Å})$ and $R_6 = I(296.13\ \text{Å})/I(349.87\ \text{Å})$, where I is in energy units, plotted as a function of logarithmic electron density (N_e in cm^{-3}) at the temperature of maximum Si IX fractional abundance in ionization equilibrium, $T_e = 1.25 \times 10^6$ K (Mazzotta *et al.*, 1998). The present calculations are shown as *solid lines*, while results from the CHIANTI Version 13 database are given as *filled circles* (R_2), *stars* (R_4), and *diamonds* (R_6).

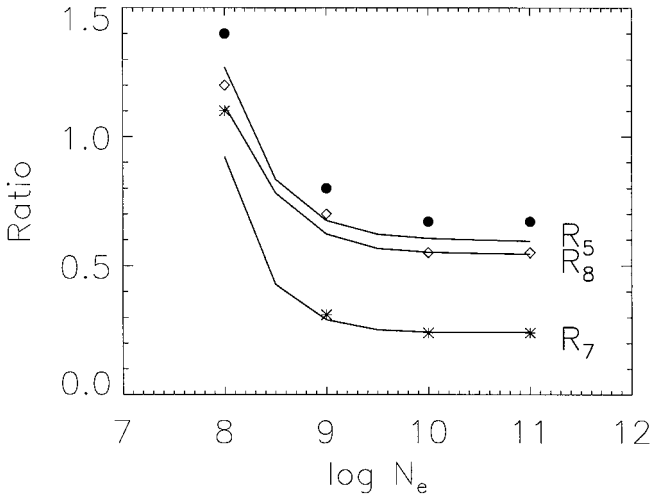

Figure 3. The theoretical Si IX emission line ratios $R_5 = I(292.80\ \text{Å})/I(349.87\ \text{Å})$, $R_7 = I(341.97\ \text{Å})/I(349.87\ \text{Å})$ and $R_8 = I(345.13\ \text{Å})/I(349.87\ \text{Å})$, where I is in energy units, plotted as a function of logarithmic electron density (N_e in cm^{-3}) at the temperature of maximum Si IX fractional abundance in ionization equilibrium, $T_e = 1.25 \times 10^6$ K (Mazzotta *et al.*, 1998). The present calculations are shown as *solid lines*, while results from the CHIANTI Version 13 database are given as *filled circles* (R_5), *stars* (R_7), and *diamonds* (R_8).

TABLE I

Si IX transitions and line-ratio designations.

Transition	λ (Å)	$R = I(\lambda)/I(349.87$ Å)
$2s^2 2p^2\ ^3P_0 - 2s2p^3\ ^3S_1$	223.74	R_1
$2s^2 2p^2\ ^3P_1 - 2s2p^3\ ^3S_1$	225.02	R_9
$2s^2 2p^2\ ^3P_2 - 2s2p^3\ ^3S_1$	227.00	R_{10}
$2s^2 2p^2\ ^1D_2 - 2s2p^3\ ^1P_1$	227.36	R_{14}
$2s^2 2p^2\ ^1D_2 - 2s2p^3\ ^1D_2$	258.10	R_2
$2s^2 2p^2\ ^1S_0 - 2s2p^3\ ^1P_1$	259.77	R_3
$2s^2 2p^2\ ^3P_0 - 2s2p^3\ ^3P_1$	290.69	R_4
$2s^2 2p^2\ ^3P_1 - 2s2p^3\ ^3P_{0,1,2}$	292.80	R_5
$2s^2 2p^2\ ^3P_2 - 2s2p^3\ ^3P_2$	296.13	R_6
$2s^2 2p^2\ ^3P_2 - 2s2p^3\ ^3P_1$	296.23	R_{11}
$2s^2 2p^2\ ^3P_0 - 2s2p^3\ ^3D_1$	341.97	R_7
$2s^2 2p^2\ ^3P_1 - 2s2p^3\ ^3D_1$	344.96	R_{12}
$2s^2 2p^2\ ^3P_1 - 2s2p^3\ ^3D_2$	345.13	R_8
$2s^2 2p^2\ ^3P_2 - 2s2p^3\ ^3D_1$	349.62	R_{13}
$2s^2 2p^2\ ^3P_2 - 2s2p^3\ ^3D_{2,3}$	349.87	–

In Figures 1–3 we plot the theoretical emission line ratios

$R_1 = I(223.74$ Å$)/I(349.87$ Å$)$,
$R_2 = I(258.10$ Å$)/I(349.87$ Å$)$,
$R_3 = I(259.77$ Å$)/I(349.87$ Å$)$,
$R_4 = I(290.69$ Å$)/I(349.87$ Å$)$,
$R_5 = I(292.80$ Å$)/I(349.87$ Å$)$,
$R_6 = I(296.13$ Å$)/I(349.87$ Å$)$,
$R_7 = I(341.97$ Å$)/I(349.87$ Å$)$,
and
$R_8 = I(345.13$ Å$)/I(349.87$ Å$)$

as functions of logarithmic electron density at the electron temperature of maximum Si IX fractional abundance in ionization equilibrium, $T_{\max} = 1.25 \times 10^6$ K (Mazzotta *et al.*, 1998). The transitions corresponding to these wavelengths are listed in Table I. Given errors in the adopted atomic data of typically $\pm 10\%$ (see above references), we would expect the theoretical ratios to be accurate to better than $\pm 15\%$.

We note that the ratios

$R_9 = I(225.02\ \text{Å})/I(349.87\ \text{Å})$,
$R_{10} = I(227.00\ \text{Å})/I(349.87\ \text{Å})$,
$R_{11} = I(296.23\ \text{Å})/I(349.87\ \text{Å})$,
$R_{12} = I(344.96\ \text{Å})/I(349.87\ \text{Å})$,
$R_{13} = I(349.62\ \text{Å})/I(349.87\ \text{Å})$,
and
$R_{14} = I(227.36\ \text{Å})/I(349.87\ \text{Å})$

have the same temperature and density dependence as R_1, R_3, R_4 and R_7 owing to common upper levels, but with

$R_9 = 2.99 \times R_1$,
$R_{10} = 5.08 \times R_1$,
$R_{11} = 1.17 \times R_4$,
$R_{12} = 0.581 \times R_7$,
$R_{13} = 0.0239 \times R_7$,
and
$R_{14} = 4.69 \times R_3$.

An inspection of Figures 1–3 reveals that the ratios are sensitive to variations in the electron density, with for example R_2 and R_3 varying by factors of 14 and 20, respectively, between $N_e = 10^8$ and 10^{11} cm^{-3}. However we note that the ratios are relatively insensitive to changes in the adopted electron temperature. For example, increasing T_e from 1.25×10^6 K to 2×10^6 K (i.e., by 60%) leads to only a 20%, 6%, and 4% variation in R_1, R_2, and R_3, respectively, at $N_e = 10^8$ cm^{-3}. At $N_e = 10^{10}$ cm^{-3}, the changes due to the temperature increase are still only 12% (R_1), 24% (R_2), and 23% (R_3). This sensitivity to changes in the electron density, but not temperature, indicates that the ratios should (in principle) be useful N_e-diagnostics for the Si IX emitting region of a plasma.

Also shown in Figures 1–3 are the theoretical line ratios generated using the CHIANTI Version 13 database (Landi *et al.*, 1999, and references therein), which differ by up to 60% from those presented here. These discrepancies are due primarily to the use in CHIANTI of electron impact excitation rates for $2s^2 2p^2 - 2s2p^3$ and $2s2p^3 - 2s2p^3$ transitions from Bhatia and Doschek (1993) calculated in the Distorted-Wave approximation, which does not consider resonance structure. By contrast, the R-matrix calculations of Aggarwal (1984) and Aggarwal and Kingston (1986) include an explicit delineation of the resonance structure in the collision cross sections. In addition, we note that the CHIANTI results do not include the effects of proton excitation as of Version 13, and so our new calculations need to be incorporated into future versions of its database.

TABLE II

Si IX emission line ratios in the SERTS-89 observations[a].

Ratio	Active region		Subflare	
	Observed[b]	Theoretical[c]	Observed[d]	Theoretical[e]
R_2	0.38 ± 0.15	0.30 ± 0.05	0.32 ± 0.12	0.40 ± 0.06
R_3	0.13 ± 0.10	0.03 ± 0.01	–	0.04 ± 0.01
R_4	0.24 ± 0.12	0.19 ± 0.03	0.22 ± 0.12	0.19 ± 0.03
R_5	0.50 ± 0.12	0.61 ± 0.09	0.48 ± 0.16	0.60 ± 0.09
R_6	1.0 ± 0.1	0.81 ± 0.12	0.54 ± 0.21	0.80 ± 0.12
R_7	0.21 ± 0.04	0.25 ± 0.04	0.16 ± 0.07	0.24 ± 0.04
R_8	0.50 ± 0.05	0.56 ± 0.08	0.45 ± 0.11	0.55 ± 0.08
R_{11}	0.26 ± 0.04	0.22 ± 0.03	0.28 ± 0.14	0.22 ± 0.03
R_{12}	0.12 ± 0.04	0.15 ± 0.02	0.18 ± 0.06	0.14 ± 0.02

[a]The first-order SERTS-89 bandpass is 235.5–448.7 Å.
[b]$I(349.87\ \text{Å}) = 139.8 \pm 5.8$ erg cm^{-2} s^{-1} sr^{-1}.
[c]Determined from Figures 1–3 at $N_e = 10^{9.7}$ cm^{-3}.
[d]$I(349.87\ \text{Å}) = 209.6 \pm 21.5$ erg cm^{-2} s^{-1} sr^{-1}.
[e]Determined from Figures 1–3 at $N_e = 10^{9.9}$ cm^{-3}.

3. Observational Data

The solar spectra analysed in the present paper are those of several quiet and active regions, a small subflare, and an off-limb area, obtained with the SERTS instrument (Neupert *et al.*, 1992). These spectra were recorded on Eastman Kodak 101-07 emulsion by SERTS during rocket flights on 5 May 1989 at 17:45 UT (SERTS-89), 7 May 1991 at 18:05 UT (SERTS-91), 17 August 1993 at 18:00 UT (SERTS-93) and 15 May 1995 at 18:00 UT (SERTS-95). For the rocket flight on 18 November 1997 at 19:35 UT (SERTS-97), an intensified CCD was employed as the detector. The spectral resolutions of the SERTS datasets are typically 50–80 mÅ (FWHM), apart from the SERTS-97 observations which have a resolution of 115 mÅ, while the spatial resolutions are about 7 arc sec (FWHM). Further details of the observations, and the wavelength and absolute flux calibration procedures employed in the data reduction, may be found in the following papers – SERTS-89: Thomas and Neupert (1994); SERTS-91 and SERTS-93: Brosius *et al.* (1996); SERTS-95: Brosius, Davila, and Thomas (1998); SERTS-97: Brosius *et al.* (2000).

Table I lists all of the strongest emission features of Si IX occurring between 220–350 Å, a spectral range largely covered by numerous flights of the SERTS rocket spectrograph. Intensities of these features (where measurable) were determined by using the spectrum synthesis package DIPSO (Howarth, Murray, and Mills, 1994) to fit gaussian profiles to the SERTS observations. The intensities of the 349.87 Å line are listed as footnotes to Tables II–VII; the observed intensities

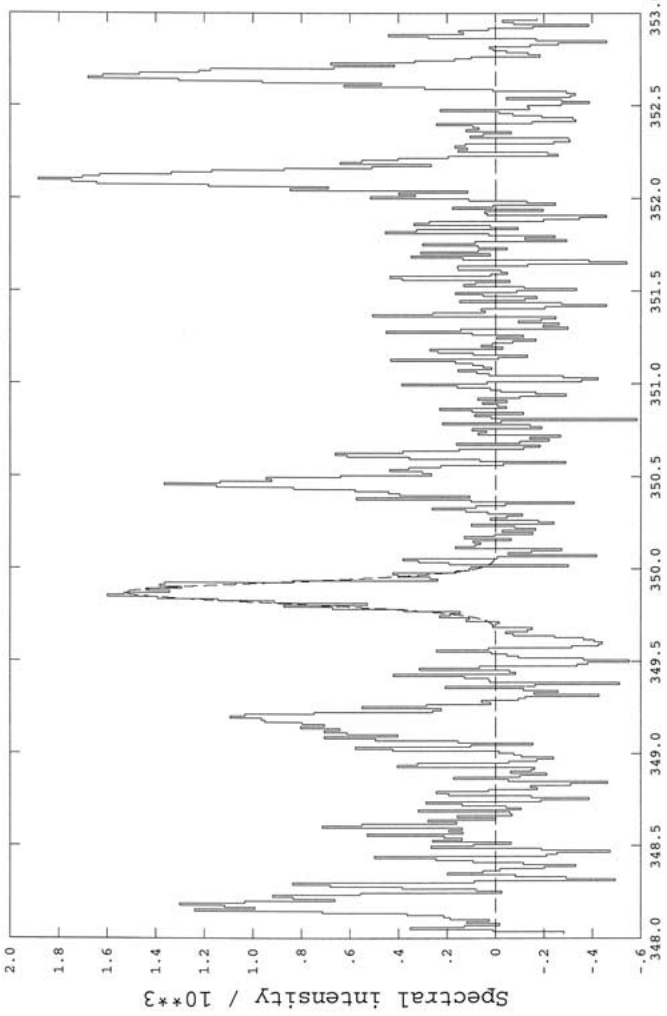

Figure 4. Plot of the SERTS-89 subflare spectrum in the 348.0–353.0 Å wavelength range, where the spectral intensity is in units of erg cm^{-2} s^{-1} sr^{-1} $Å^{-1}$. The profile fit to the Si IX 349.87 Å feature is shown by a *dashed line*. Also clearly visible in the figure are the Fe XIII 348.20 Å, Mg VI 349.12 Å, Fe XVII 350.52 Å, Fe XII 352.13 Å and Fe XI 352.70 Å emission lines.

TABLE III

Si IX emission line ratios in the SERTS-91 active-region and quiet-Sun observations[a].

Ratio	Active region		Quiet Sun	
	Observed[b]	Theoretical[c]	Observed[d]	Theoretical[e]
R_4	0.33 ± 0.06	0.20 ± 0.03	0.12 ± 0.07	0.22 ± 0.03
R_5	0.34 ± 0.18	0.62 ± 0.09	0.56 ± 0.28	0.67 ± 0.10
R_6	0.89 ± 0.23	0.81 ± 0.12	0.59 ± 0.10	0.83 ± 0.12
R_7	0.29 ± 0.06	0.25 ± 0.04	0.34 ± 0.18	0.29 ± 0.04
R_8	0.62 ± 0.07	0.57 ± 0.09	0.53 ± 0.04	0.62 ± 0.09
R_{11}	0.44 ± 0.23	0.23 ± 0.03	0.13 ± 0.08	0.26 ± 0.04
R_{12}	0.16 ± 0.06	0.15 ± 0.02	0.16 ± 0.05	0.17 ± 0.03

[a]The first-order SERTS-91 bandpass is 231.8–445.3 Å.
[b]$I(349.87\ \text{Å}) = 45.0 \pm 2.2$ erg cm^{-2} s^{-1} sr^{-1}.
[c]Determined from Figures 1–3 at $N_e = 10^{9.6}$ cm^{-3}.
[d]$I(349.87\ \text{Å}) = 121.8 \pm 4.1$ erg cm^{-2} s^{-1} sr^{-1}.
[e]Determined from Figures 1–3 at $N_e = 10^{9}$ cm^{-3}.

TABLE IV

Si IX emission line ratios in the SERTS-91 off-limb observations[a].

Ratio	Observed[b]	Theoretical[c]
R_4	0.12 ± 0.04	0.22 ± 0.03
R_5	0.35 ± 0.11	0.66 ± 0.10
R_6	0.76 ± 0.09	0.83 ± 0.12
R_7	0.49 ± 0.05	0.28 ± 0.04
R_8	0.69 ± 0.07	0.61 ± 0.09
R_{11}	0.22 ± 0.05	0.26 ± 0.04
R_{12}	0.18 ± 0.09	0.16 ± 0.02

[a]The first-order SERTS-91 bandpass is 231.8–445.3 Å.
[b]$I(349.87\ \text{Å}) = 200.1 \pm 12.5$ erg cm^{-2} s^{-1} sr^{-1}.
[c]Determined from Figures 1–3 at $N_e = 10^{9.1}$ cm^{-3}.

of the other Si IX transitions may be inferred from these using the line ratios given in the tables (see Section 2). Also given as footnotes to the tables are the first-order bandpasses of the SERTS datasets.

Observational uncertainties in the line intensities have been determined using methods discussed in detail by Thomas and Neupert (1994). The intensities and uncertainties quoted here are somewhat different from those originally reported in the papers referenced above, because the spectral data have been completely re-analysed by a standard fitting procedure to assure consistency of the results.

TABLE V

Si IX emission line ratios in the SERTS-93 observations[a].

Ratio	Active region		Quiet Sun	
	Observed[b]	Theoretical[c]	Observed[d]	Theoretical[e]
R_4	0.10 ± 0.05	0.19 ± 0.03	0.14 ± 0.05	0.22 ± 0.03
R_5	0.36 ± 0.12	0.61 ± 0.09	0.64 ± 0.17	0.67 ± 0.10
R_6	–	0.81 ± 0.12	0.71 ± 0.08	0.83 ± 0.12
$R_6 + R_{11}$	1.4 ± 0.1	1.0 ± 0.2	–	1.1 ± 0.2
R_7	0.22 ± 0.02	0.25 ± 0.04	0.30 ± 0.02	0.29 ± 0.04
R_8	0.63 ± 0.03	0.56 ± 0.08	0.65 ± 0.04	0.62 ± 0.09
R_{11}	–	0.22 ± 0.03	0.09 ± 0.05	0.26 ± 0.04
R_{12}	0.09 ± 0.04	0.15 ± 0.02	0.16 ± 0.03	0.17 ± 0.03

[a]The first-order SERTS-93 bandpass is 231.7–445.4 Å.
[b]$I(349.87\ \text{Å}) = 197.3 \pm 5.3$ erg cm^{-2} s^{-1} sr^{-1}.
[c]Determined from Figures 1–3 at $N_e = 10^{9.7}$ cm^{-3}.
[d]$I(349.87\ \text{Å}) = 46.9 \pm 0.9$ erg cm^{-2} s^{-1} sr^{-1}.
[e]Determined from Figures 1–3 at $N_e = 10^{9}$ cm^{-3}.

TABLE VI

Si IX emission line ratios in the SERTS-95 active-region observations[a].

Ratio	Observed[b]	Theoretical[c]
R_2	0.18 ± 0.10	0.18 ± 0.03
R_4	0.19 ± 0.09	0.20 ± 0.03
R_5	0.76 ± 0.20	0.63 ± 0.09
R_6	1.1 ± 0.3	0.81 ± 0.12
R_7	0.32 ± 0.10	0.26 ± 0.04
R_8	0.38 ± 0.22	0.58 ± 0.09
R_{11}	0.76 ± 0.32	0.23 ± 0.03
R_{12}	0.40 ± 0.16	0.15 ± 0.02

[a]The first-order SERTS-95 bandpass is 234.1–447.7 Å. However we note that the intensity calibration is uncertain for wavelengths greater than 340 Å (see Brosius, Davila, and Thomas, 1998).
[b]$I(349.87\ \text{Å}) = 166.8 \pm 35.2$ erg cm^{-2} s^{-1} sr^{-1}.
[c]Determined from Figures 1–3 at $N_e = 10^{9.4}$ cm^{-3}.

Also, a uniform factor of 1.24 has been applied here to all SERTS-89 intensities, reflecting a more recent re-evaluation of its absolute calibration scale. Even so, in all directly comparable cases, the resulting intensity ratios differ only slightly from those obtained using previously published data.

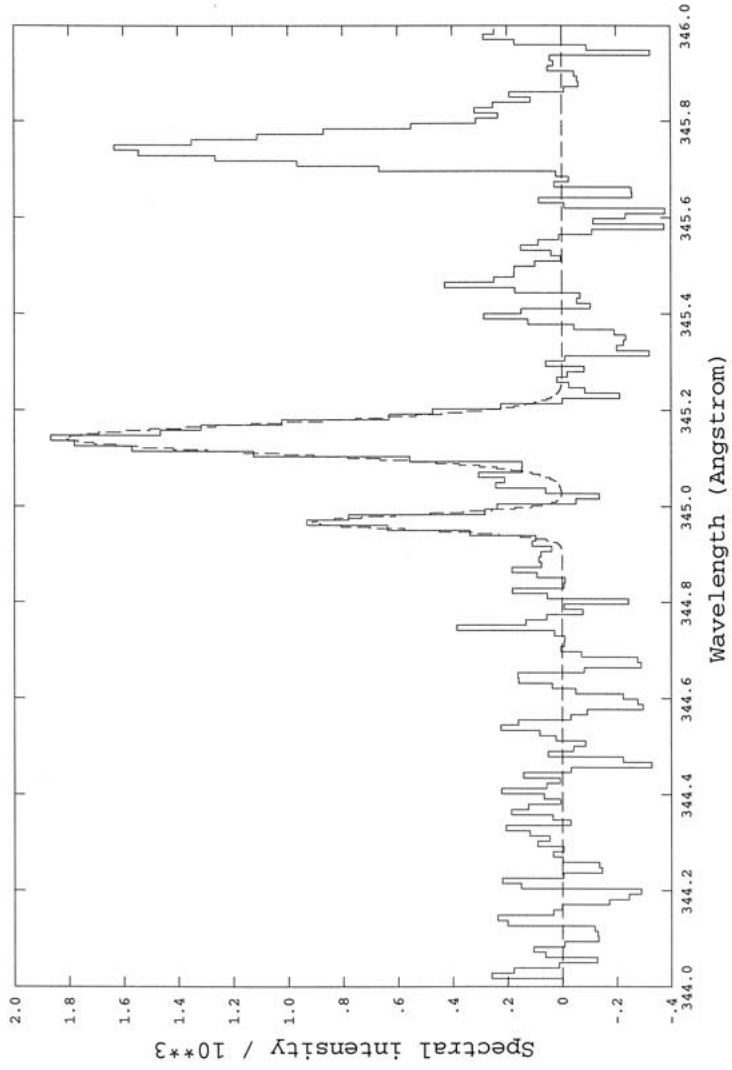

Figure 5. Plot of the SERTS-91 off-limb spectrum in the 344.0–346.0 Å wavelength range, where the spectral intensity is in units of erg cm^{-2} s^{-1} sr^{-1} $Å^{-1}$. Profile fits to the Si IX 344.96 Å and 345.13 Å features are shown by a *dashed line*. Also clearly visible in the figure is the Fe X 345.75 Å emission line.

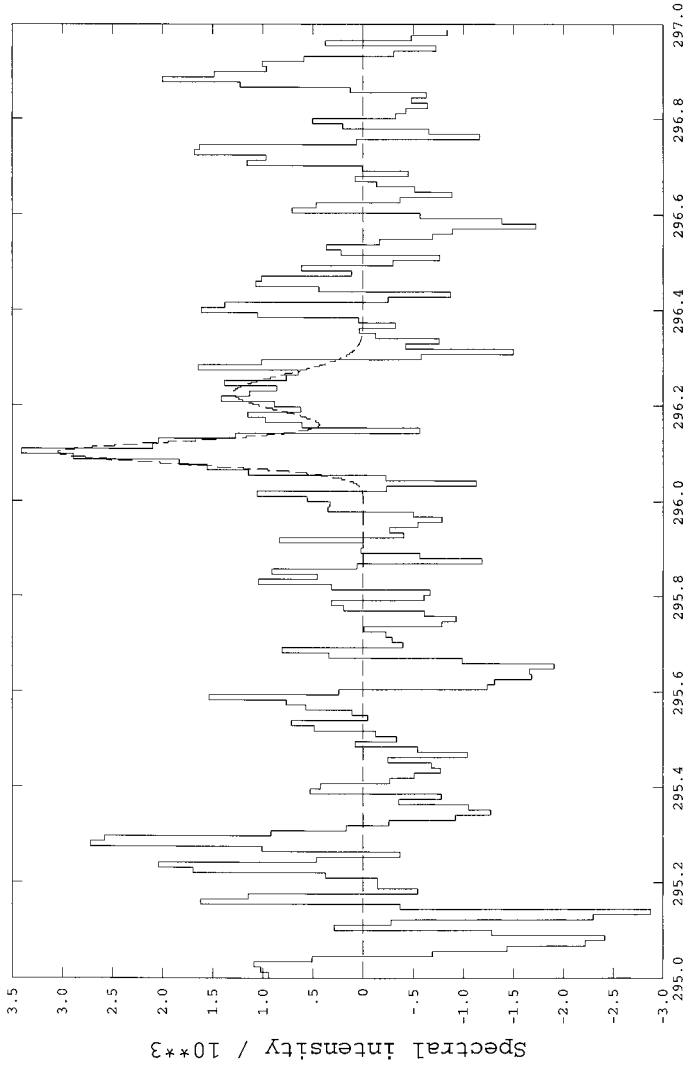

Figure 6. Plot of the SERTS-95 active region spectrum in the 295.0–297.0 Å wavelength range, where the spectral intensity is in units of erg cm^{-2} s^{-1} sr^{-1} Å^{-1}. The double gaussian profile fit to the Si IX 296.13 and 296.23 Å features is shown by a *dashed line*.

TABLE VII

Si IX emission line ratios in the SERTS-97 observations[a].

Ratio	Active region		Quiet Sun	
	Observed[b]	Theoretical[c]	Observed[d]	Theoretical[e]
R_7	0.23 ± 0.05	0.25 ± 0.04	0.20 ± 0.04	0.29 ± 0.04
R_8	0.59 ± 0.13	0.56 ± 0.08	0.60 ± 0.13	0.62 ± 0.09
R_{12}	0.13 ± 0.03	0.15 ± 0.02	0.15 ± 0.08	0.17 ± 0.03

[a]The first-order SERTS-97 bandpass is 299.0–353.5 Å.
[b]$I(349.87\ \text{Å}) = 121.5 \pm 18.2$ erg cm^{-2} s^{-1} sr^{-1}.
[c]Determined from Figures 1–3 at $N_e = 10^{9.7}$ cm^{-3}.
[d]$I(349.87\ \text{Å}) = 39.2 \pm 5.9$ erg cm^{-2} s^{-1} sr^{-1}.
[e]Determined from Figures 1–3 at $N_e = 10^{9}$ cm^{-3}.

The quality of the Si IX observational data are illustrated in Figures 4–7, where we plot several portions of the SERTS spectra for a variety of solar features measured on different flights of the rocket payload.

4. Results and Discussion

In Tables II–VII we list the observed Si IX emission line ratios measured from the SERTS spectra, along with the associated 1σ errors. Young, Landi, and Thomas (1998) first pointed out that the Si IX feature at 296.14 Å in the SERTS-89 active region spectrum could be resolved into two lines at 296.13 and 296.23 Å. We have been able to resolve these lines in most of the SERTS spectra (see, for example, Figure 6), and hence measure the R_6 and R_{11} ratios. However, for the SERTS-93 active-region observations the 296.13 and 296.23 Å lines could not be resolved, and hence for this spectrum we have determined only the $R_6 + R_{11}$ ratio.

Also shown in Tables II–VII are the theoretical results from Figures 1–3 at electron densities derived for the SERTS solar features from emission line ratios in Fe XII or Fe XIII (Keenan *et al.*, 1996; Brosius *et al.*, 1996, 1998). These species have temperatures of maximum fractional abundance in ionization equilibrium of $T_{\max}$ (Fe XII) $= 1.5 \times 10^6$ K and $T_{\max}$ (Fe XIII) $= 1.6 \times 10^6$ K (Mazzotta *et al.*, 1998), very close to that for Si IX. Hence the Fe XII and Fe XIII densities should reflect that of the Si IX emitting plasma in the solar feature. The error bars on the theoretical results are based on the estimated $\pm 15\%$ accuracy of the line-ratio calculations (see Section 2).

An inspection of Tables II–VII reveals generally very good agreement between theory and observation. For many of the line ratios, the observational uncertainties are around 20–30%, but several are accurate to 10% or better (for example, R_7 and R_8 in the SERTS-93 active-region spectrum). The agreement between theory and experiment for these measurements, in particular, provides support for the

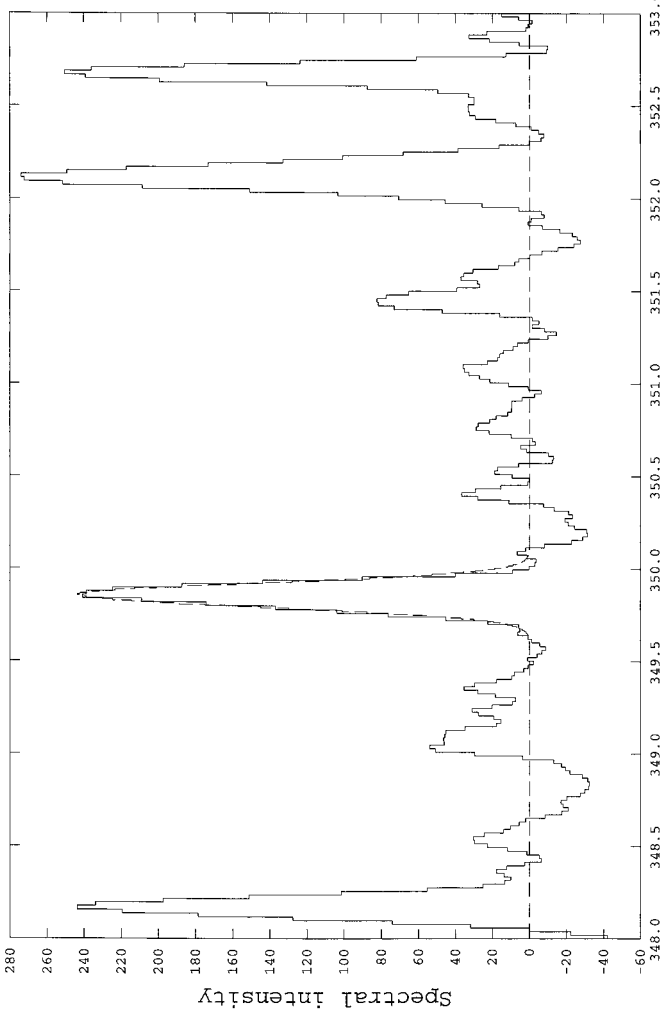

Figure 7. Plot of the SERTS-97 quiet-Sun spectrum in the 348.0–353.0 Å wavelength range, where the spectral intensity is in units of erg cm^{-2} s^{-1} sr^{-1} $Å^{-1}$. The profile fit to the Si IX 349.87 Å feature is shown by a *dashed line*. Also clearly visible in the figure are the Fe XIII 348.20 Å, Fe XII 352.13 Å and Fe XI 352.70 Å emission lines.

accuracy of the line-ratios calculations, and hence the atomic data on which they are based. They may therefore be applied with confidence to the analysis of solar observations, or other remote astrophysical sources such as late-type stars. In particular, the ratio $R_2 = I(258.10\ \text{Å})/I(349.87\ \text{Å})$ appears to provide an especially promising diagnostic of coronal plasma densities, as it involves two reasonably strong emission lines and varies by more than an order of magnitude over the very useful density range of $10^9 - 10^{11}$ cm^{-3} (see Figure 2). However, care must be taken to ensure that the Si IX 258.10 Å line is well resolved from nearby Si X 258.37 Å emission when using this ratio.

In addition to the generally excellent agreement between theory and observation for the measured line intensities in Tables II–VII, we note that all non-detections are also consistent with our theoretical results. For the non-detections, the line is either outside the first-order bandpass of the corresponding SERTS dataset, or else its predicted intensity is well below the instrument's 3σ sensitivity level at that wavelength.

Finally, we note that we have obtained a very marginal detection of the Si IX 259.77 Å line in the SERTS-89 active-region spectrum. The resultant R_3 ratio in Table II agrees with theory, although the error bar on the measured value is very large. If real, this is the first detection of the 259.77 Å feature in the SERTS spectral database, although we note that the line has been observed in solar flare spectra from *Skylab* (Dere, 1978).

Acknowledgements

ACK acknowledges financial support from the Leverhulme Trust via grant F/00203/A. The SERTS rocket programme is funded under NASA RTOP 344–17–38. JWB acknowledges additional NASA support under contract NAS5–99145.

References

Aggarwal, K. M.: 1983, *J. Phys.* **B16**, L59.
Aggarwal, K. M.: 1984, *Astrophys. J. Suppl.* **54**, 1.
Aggarwal, K. M.: 1998, *Astrophys. J. Suppl.* **118**, 589.
Aggarwal, K. M. and Kingston, A. E.: 1986, *Astron. Astrophys.* **162**, 333.
Bhatia, A. K. and Doschek, G. A.: 1993, *Atomic Data Nucl. Data Tables* **55**, 281.
Brage, T., Judge, P. G., Jönsson, P., and Edwards, D. P.: 2000, *Astrophys. J.* **540**, 1114.
Brosius, J. W., Davila, J. M., and Thomas, R. J.: 1998, *Astrophys. J. Suppl.* **119**, 255.
Brosius, J. W., Davila, J. M., Thomas, R. J., and Monsignori-Fossi, B. C.: 1996, *Astrophys. J. Suppl.* **106**, 143.
Brosius, J. W., Thomas, R. J., Davila, J. M., and Landi, E.: 2000, *Astrophys. J.* **543**, 1016.
Dere, K. P.: 1978, *Astrophys. J.* **221**, 1062.
Dufton, P. L.: 1977, *Comp. Phys. Comm.* **13**, 25.
Dufton, P. L., Berrington, K. A., Burke, P. G., and Kingston, A. E.: 1978, *Astron. Astrophys.* **62**, 111.

Gallagher, P. T., Mathioudakis, M., Keenan, F. P., Phillips, K. J. H., and Tsinganos, K.: 1999, *Astrophys. J.* **524**, L133.

Gallagher, P. T., Phillips, K. J. H., Lee, J., Keenan, F. P., and Pinfield, D. J.: 2001, *Astrophys. J.* **558**, 411.

Howarth, I. D., Murray, J., and Mills, D.: 1994, *Starlink User Note No. 50.15*.

Keenan, F. P.: 1996, *Space Sci. Rev.* **75**, 537.

Keenan, F. P., Thomas, R. J., Neupert, W. M., Foster, V. J., Brown, P. J. F., and Tayal, S. S.: 1996, *Monthly Notices Royal Astron. Soc.* **278**, 773.

Landi, E., Landini, M., Dere, K. P., Young, P. R., and Mason, H. E.: 1999, *Astron. Astrophys. Suppl.* **135**, 339.

Martin, W. C. and Zalubas, R.: 1983, *J. Phys. Chem. Ref. Data* **12**, 366.

Mason, H. E. and Bhatia, A. K.: 1978, *Monthly Notices Royal Astron. Soc.* **184**, 423.

Mazzotta, P., Mazzitelli, G., Colafrancesco, S., and Vittorio, N.: 1998, *Astron. Astrophys. Suppl.* **133**, 403.

Neupert, W. M., Epstein, G. L., Thomas, R. J., and Thompson, W. T.: 1992, *Solar Phys.* **137**, 87.

Ryans, R. S. I., Foster-Woods, V. J., Keenan, F. P., and Reid, R. H. G.: 1999, *Atomic Data Nucl. Data Tables* **73**, 1.

Thomas, R. J. and Neupert, W. M.: 1994, *Astrophys. J. Suppl.* **91**, 461.

Young, P. R., Landi, E., and Thomas, R. J.: 1998, *Astron. Astrophys.* **329**, 291.